Suppression of the charge density wave instability in R_2O_2Bi (R = La, Er) due to large spin-orbit coupling

Heejung Kim,[1] Chang-Jong Kang,[1] Kyoo Kim,[1,2] J. H. Shim,[3,*] and B. I. Min[1,†]
[1]*Department of physics, Pohang University of Science and Technology, Pohang 37673, Korea*
[2]*c-CCMR, Pohang University of Science and Technology, Pohang 37673, Korea*
[3]*Department of chemistry and Division of Advanced Nuclear Engineering, Pohang University of Science and Technology, Pohang 37673, Korea*
(Received 13 November 2015; revised manuscript received 9 February 2016; published 9 March 2016)

To explore the origin of the suppression of the charge density wave (CDW) in Bi^{2-} square sheet of R_2O_2Bi (R: rare-earth elements), we have investigated the band structures and phonon dispersions of La_2O_2Bi and Er_2O_2Bi. We have found that the large spin-orbit coupling of Bi atoms together with the chemical pressure effect reduces the Fermi surface nesting, which results in the suppression of the CDW instability in R_2O_2Bi. The pressure effect has been checked for a similar compound, Er_2O_2Sb, which shows a series of structural distortions in the Sb layer under volume contraction, from herringbone type, to 1D-ladder type, and to square sheet. Furthermore, we show that the observed local disorder in the Bi square sheet of La_2O_2Bi can be explained by the phonon softening anomaly, which is also expected to describe the anomalous resistivity upturn observed in La_2O_2Bi upon cooling.

DOI: 10.1103/PhysRevB.93.125116

I. INTRODUCTION

A two-dimensional (2D) square sheet in pnictides (Pn) usually forms an electron-rich network with the valence state of $Pn^{1-}(s^2p^4)$ which is explained by the hypervalent scheme [1]. The structure containing the hypervalent bonding is often changed into a lower dimensional structure by the charge density wave (CDW) or Peierls-like instability. Such distorted square sheets are reported for $EuSb_2$ [2], $CaSb_2$, and $SrZnSb_2$ having a zigzag type, and GdPS having a ladder type [3]. However, some Pn square sheets are not distorted by the CDW instability. For example, $YbSb_2$ has a Sb square sheet albeit slightly puckered [4], and $BaZnSb_2$ maintains the Sb square sheet [5]. Also, the materials with Bi, such as $SrZnBi_2$, $SrMnBi_2$ [6], $CeNiBi_2$ [7], and $EuBi_2$ [8], retain the original square sheet.

The structural transition of a 2D square sheet in Pn has been explored earlier by Papoian and Hoffman [9]. They suggested that the separation in energy between the Pn-p states and the cation d states produces the distortion of the square sheet. For example, the bands from Sb square sheets in $CaSb_2$ and $SrZnSb_2$ are well separated from other metallic bands, and so the distorted structure is preferred. But this is not always the case. In $EuSb_2$, the Sb square sheet experiences the distortion even though Sb p and Eu d states are close enough to be mixed. Therefore, it is more plausible to expect that the distortion arises from the CDW transition induced by the Fermi surface (FS) nesting [10].

It was recently reported that the Seebeck coefficient and the electrical conductivity of R_2O_2Sb (R = rare-earth element) are enhanced simultaneously by changing R [11]. Interestingly, in this case, the occupancy of Sb is s^2p^5 (Sb^{2-}). As mentioned above, Pn^{1-} can maintain the square sheet, but Pn^{2-} usually forms a dimer satisfying the octet rule or one-dimensional (1D) linear chain with a hypervalent bonding [9]. In the aspect of molecular bonding, the Pn^{2-} square sheets should be unstable because the antibonding states are partially occupied.

Indeed, x-ray diffraction experiments on R_2O_2Sb systems show the anisotropic pattern, which can be understood based on the formation of Sb dimer [11–13]. In our previous work [10] we showed that the Sb square sheet in R_2O_2Sb becomes distorted to have herringbone-type Sb dimers [see Fig. 5(b)]. We also demonstrated that this distortion arises from the CDW instability induced by the FS nesting. Accordingly, all R_2O_2Sb systems are insulators through the CDW band gap opening in the Sb p bands near the Fermi level (E_F).

In contrast, R_2O_2Bi has been reported to show no structural transition. Namely, the Bi^{2-} square sheet seems to be retained in R_2O_2Bi. The Bi atom in R_2O_2Bi shows the anisotropy of thermal motion suggesting the local disorder, but the size of local disorder is much smaller than that in R_2O_2Sb [14]. Hence most of R_2O_2Bi exhibits the metallic behavior except for La_2O_2Bi [15]. The most intriguing feature is that the resistivity of La_2O_2Bi shows a slight upturn with decreasing temperature, indicating the insulating behavior. This upturn in La_2O_2Bi was suggested to be related to either a grain boundary effect [12] or a Mott transition effect [15]. Thus it is still an important issue whether the Bi^{2-} square sheet in R_2O_2Bi is really retained or not. Furthermore, the variation in the resistivity due to the chemical pressure effect of R ion also remains to be investigated.

In this work we have investigated the structural properties of R_2O_2Bi (R with La and Er) in comparison to those of R_2O_2Sb. The electronic band structures and phonon dispersions of R_2O_2Bi were calculated to understand the origin of a seemingly stable Bi square sheet. We have shown that the stable Bi^{2-} square sheet can be explained by the large spin-orbit coupling (SOC) and orbital overlap of the extended Bi orbital. We have also found that slight local disorder of Bi atoms in La_2O_2Bi can be realized with negligible energy loss of 0.7 meV for about 0.1 Å distortion. In addition, we have shown that the phonon dispersion in the pressurized R_2O_2Sb is quite similar to that in R_2O_2Bi, which demonstrates the

*jhshim@postech.ac.kr
†bimin@postech.ac.kr

 ©2016 American Physical Society

TABLE I. Experimental and calculated lattice parameters (a and c) and volumes V of Er_2O_2Sb, Er_2O_2Bi, and La_2O_2Bi.

		Expt.	w/o-SOC	w-SOC
Er_2O_2Bi	a (Å)	3.845	3.851	3.863
	c (Å)	13.151	13.462	13.367
	V (Å^3)	194.46	199.72	199.43
La_2O_2Bi	a (Å)	4.085	4.087	4.103
	c (Å)	13.987	14.292	14.161
	V (Å^3)	233.37	238.78	238.44
Er_2O_2Sb	a (Å)	3.815	3.821	–
	c (Å)	13.007	13.238	–
	V (Å^3)	189.31	193.28	–

importance of orbital overlap effect of a Pn element. Based on the band structures incorporating the Coulomb correlation U of Bi p-orbital states, we showed that the Mott-type insulator cannot be realized in La_2O_2Bi. We suggested that large electron-phonon coupling (EPC) in La_2O_2Bi increases the electronic scattering, which would induce the upturn of the resistivity in decreasing temperature.

II. COMPUTATIONAL DETAILS

We have employed the Vienna *ab initio* simulation package (VASP) [16] within the generalized gradient approximation (GGA). We have also repeated the same calculation using the full-potential method implemented in WIEN2k [17]. Two sets of methods satisfy the consistency of the band structures. The electronic charge density was evaluated up to the kinetic energy cutoff of 500 eV. The Brillouin-zone (BZ) integration was carried out with $10\times10\times10$ k points for the self-consistent calculations. For the calculations of Fermi surface and charge susceptibility, $100\times100\times100$ k points were used for the BZ integration. The SOC was included in the second-variational scheme for R_2O_2Bi, but not for R_2O_2Sb because its effect is negligible. The structural optimization was done by using the Hellmann-Feynman force scheme [18]. The fully relaxed structural parameters are shown in Table I, which agrees well with experimental results (within 3% differences) [13,15]. For Er_2O_2Bi and Er_2O_2Sb we considered f orbital as core state because they do not participate in the bonding.

Phonon properties were obtained by using the frozen-phonon method implemented in PHONOPY [19]. All the phonon calculations were performed after the full relaxation of the volume and atomic positions. To obtain precise phonon dispersions, we have used the $4\times4\times1$ supercell. Here $7\times7\times7$ k points ($5\times5\times5$ k points for the SOC case) were used, and the kinetic energy cutoff was 500 eV. In order to obtain the force constants and the dynamical matrix, the Hellmann-Feynman force scheme is used.

III. RESULTS AND DISCUSSIONS

Figure 1(a) shows the crystal structure of La_2O_2Bi having $I4/mmm$ space group. It is composed of Bi square sheets and R_2O_2 layers, which are stacked alternatively along the c axis. Due to clear separation between the Bi square sheet and the R_2O_2 layer, the interaction along the c axis would be small,

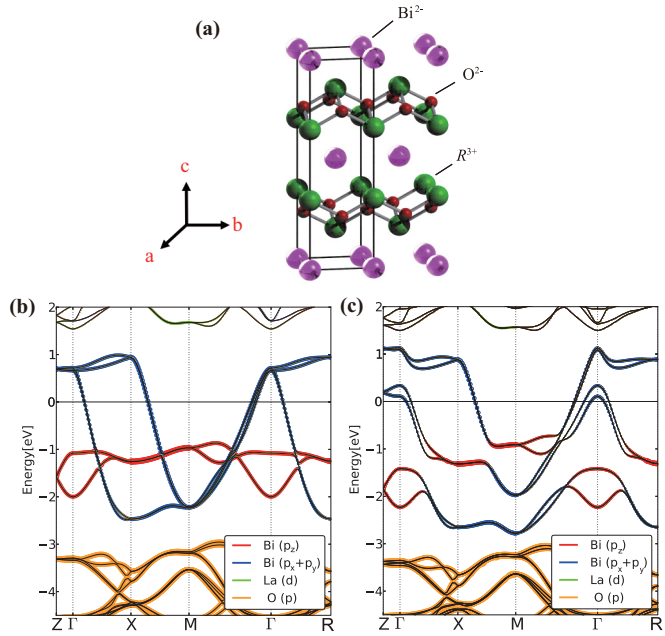

FIG. 1. (a) Tetragonal structure of R_2O_2Bi having a space group of $I4mmm$. The band structure of La_2O_2Bi along the symmetry lines of the tetragonal BZ (b) without the SOC (w/o-SOC) and (c) with the SOC (w-SOC).

and so the electron hopping would happen only in the square sheets. Due to different R atom size, the interatomic distance between Bi atoms decreases from La_2O_2Bi to Er_2O_2Bi by 5.9%. Figures 1(b) and 1(c) are the band structures of La_2O_2Bi without the SOC and with the SOC (hereafter we call w/o-SOC and w-SOC, respectively). Both band structures show 2D properties with flat dispersions along the Γ-Z direction. Oxygen $2p$ bands are well below E_F (< -3.0 eV), while La d bands are located well above E_F because La ions have typical trivalent states. So, the states near E_F are dominated by Bi $6p$ bands, which are dispersive with the bandwidth of about 3.5 eV. The obtained Bi band structure is consistent with an anticipated Bi^{2-} electronic configuration of $6s^26p^5$.

The band structure of w/o-SOC in Fig. 1(b) is similar to that reported by by Mizoguchi and Hosono [7]. However, the SOC effect should be considered in this system because Bi is a quite heavy atom. As shown in Fig. 1(c), $6p_{x,y}$ and $6p_z$ bands of Bi are mixed with each other due to the SOC. However, $6p_z$ bands of Bi are well separated from $6p_{x,y}$, and so the bands near E_F correspond to mostly $6p_{x,y}$. Also, due to the SOC, the bands near E_F correspond to mostly $6p_{3/2}$. Other R_2O_2Bi's show very similar band structures to La_2O_2Bi but with different bandwidths. For example, the bandwidth of Er_2O_2Bi is about 5.0 eV, as compared to 3.5 eV for La_2O_2Bi, which is consistent with a lanthanide contraction rule (Er_2O_2Bi has 16.7% less volume than La_2O_2Bi).

As mentioned in the Introduction, the Bi square sheet in La_2O_2Bi is retained, which is unusual because Bi^{2-} ions are expected to form a dimer structure satisfying the octet rule or linear chain with hypervalent bonding [20]. To check the electronic instability of R_2O_2Bi, we investigate the FSs and the real part of the charge susceptibility [$\chi_0(\mathbf{q})$] as shown in Fig. 2. We consider both cases with and without the

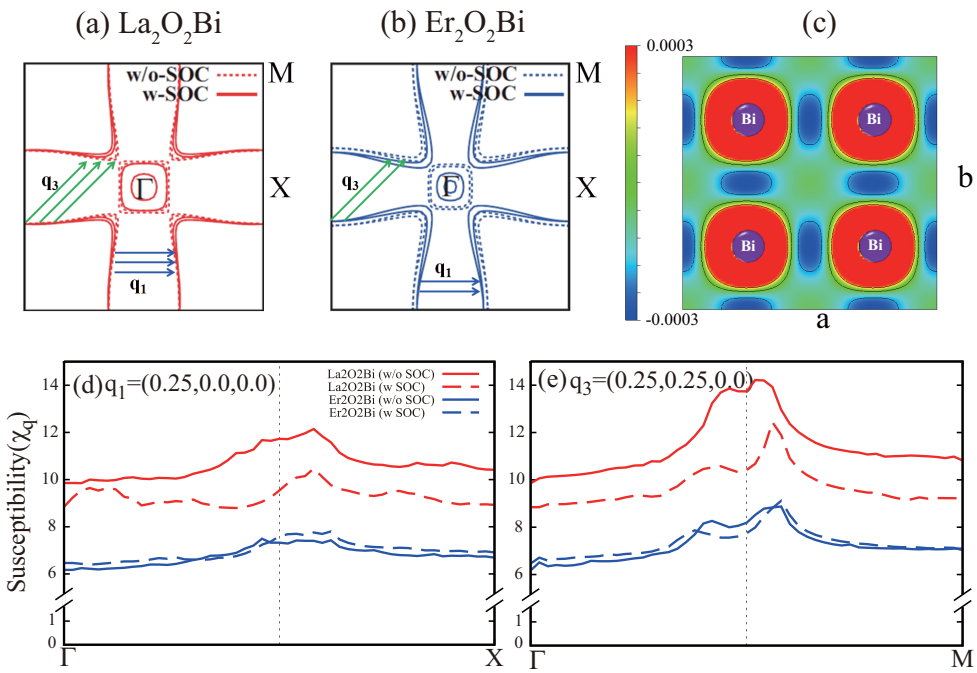

FIG. 2. FSs of (a) La_2O_2Bi and (b) Er_2O_2Bi in the w-SOC (solid lines) and w/o-SOC (dotted lines) schemes. The FS nesting features are shown with nesting vectors of $\mathbf{q}_1$ and $\mathbf{q}_3$. (c) The difference of charge densities between w-SOC and w/o-SOC schemes of La_2O_2Bi in unit of $e/\text{Å}^3$. (d) and (e) The real part of charge susceptibilities [$\chi_0(\mathbf{q})$] for La_2O_2Bi (red lines) and Er_2O_2Bi (blue lines).

consideration of the SOC. As shown in Figs. 2(a) and 2(b), both compounds show the FS nesting feature, but the FS of Er_2O_2Bi shows larger curvature than that of La_2O_2Bi. It is due to the smaller lattice parameter in Er_2O_2Bi. Because the larger curvature suppresses the FS nesting [21], the FS nesting effect is reduced with decreasing the atomic size R. This feature is clearly seen in the calculated $\chi_0(\mathbf{q})$ in Figs. 2(d) and 2(e). In both compounds, clear peak structures are shown at $\mathbf{q}_1 = (0.25,0.00,0.00)$ along ΓX, at $\mathbf{q}_2 = (0.50,0.25,0.00)$ along XM (data not shown), and at $\mathbf{q}_3 = (0.25,0.25,0.00)$ along ΓM that has the highest $\chi_0(\mathbf{q})$ value. One can notice that Er_2O_2Bi has relatively reduced peaks due to the suppressed FS nesting effects in both the w-SOC and w/o-SOC cases.

The distinguishable feature between the w-SOC and w/o-SOC cases is the large separation of Γ-centered FS from others in the former. This separation is induced by the hybridization interaction between p_x and p_y orbitals [21]. Thus the enhanced separation of the Γ-centered FS for the w-SOC case can be understood by the increased orbital overlap between p_x and p_y orbitals due to the SOC. In addition, the SOC weakens the strength of a directional bonding because the charge density is reduced along the bonding direction for the w-SOC case, as shown in Fig. 2(c). Namely, the large separation of the Γ-centered FS and the weakness of a directional bonding reduce the FS nesting effect. It is seen in Figs. 2(d) and 2(e) that $\chi_0(\mathbf{q})$ peaks are distinctly suppressed by the SOC. An interesting feature is that the SOC effect in Er_2O_2Bi is not so significant as that in La_2O_2Bi, which is attributed to the large bandwidth (5.0 eV) of Er_2O_2Bi. These results suggest that the electronic instability in the Bi square sheet of La_2O_2Bi is suppressed by the SOC, and that of Er_2O_2Bi is further diminished by the volume contraction. The suppression of CDW instability in R_2O_2Bi by the large SOC is reminiscent of that in Po that has a unique simple cubic structure in nature [22].

To examine the structural instability of R_2O_2Bi in more detail, we perform the frozen phonon calculations using the $4\times4\times1$ supercell. Figure 3 shows the phonon dispersions of La_2O_2Bi and Er_2O_2Bi for both the w/o-SOC and w-SOC cases. In the w/o-SOC scheme, the phonon anomalies, the so-called Kohn anomalies, are seen to occur along the high symmetry directions in both compounds. The striking feature in La_2O_2Bi is the appearance of the imaginary phonon frequencies at $\mathbf{q}_1$, $\mathbf{q}_2$, and $\mathbf{q}_3$, which correspond to the FS nesting vectors. Thus the phonon softening instability arises from the FS nesting. The imaginary phonon frequency is described by the renormalization of phonon frequency by the electron-phonon interaction,

$$\omega_{\mathbf{q}}^2 = \Omega_{\mathbf{q}}^2 - |g(\mathbf{q})|^2\chi_0(\mathbf{q}), \tag{1}$$

where $\omega_{\mathbf{q}}$ and $\Omega_{\mathbf{q}}$ correspond to the renormalized and bare phonon frequencies, respectively, and $g(\mathbf{q})$ is the EPC strength. The large value of $\chi_0(\mathbf{q})$ at a specific $\mathbf{q}$ would yield $\omega_{\mathbf{q}}^2 < 0$, which induces the structural instability. Phonon density of states (DOS) in Fig. 3(a) shows that the softened phonon modes arise from Bi atoms, demonstrating that the Bi square sheet is unstable. This feature clearly indicates that the Bi square sheet in La_2O_2Bi would be distorted, if the SOC effect is not considered. On the other hand, as shown in Fig. 3(b), phonons of Er_2O_2Bi are harder than those of La_2O_2Bi, and so the phonon softening instabilities disappear in the former. This feature is also implicated in the suppression of the susceptibility due to the volume contraction in Er_2O_2Sb. Hence, Er_2O_2Bi does not experience the CDW instability even for the w/o-SOC case. In the w-SOC scheme, the phonons of Er_2O_2Bi become hardened only slightly, while those of

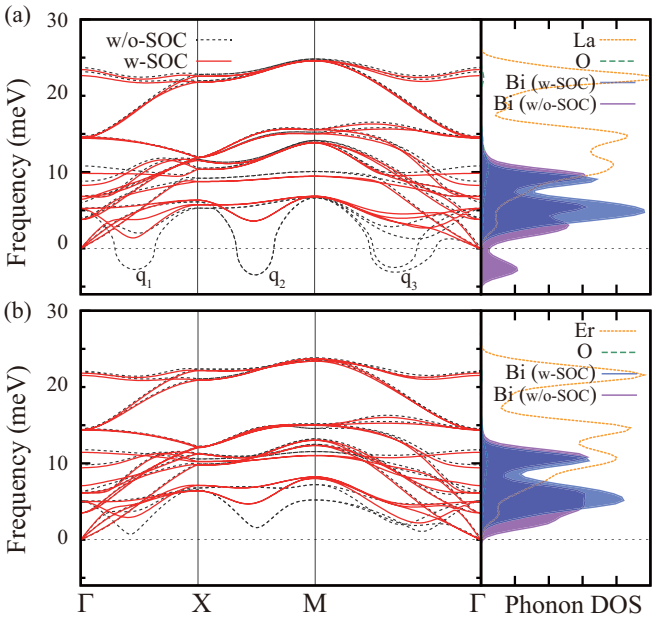

FIG. 3. Phonon dispersions and DOSs of (a) La_2O_2Bi and (b) Er_2O_2Bi in the w-SOC (solid lines) and w/o-SOC (dotted lines) schemes. The negative frequency means the imaginary value of the softened phonon frequency. There are three softened phonons at $\mathbf{q}_1$ along ΓX, at $\mathbf{q}_2$ along XM, and at $\mathbf{q}_3$ along ΓM for the w/o-SOC. Partial DOS's from La (Er) and O atoms are not affected much by inclusion of the SOC. However, the DOS from Bi atom shows significant variation by the SOC.

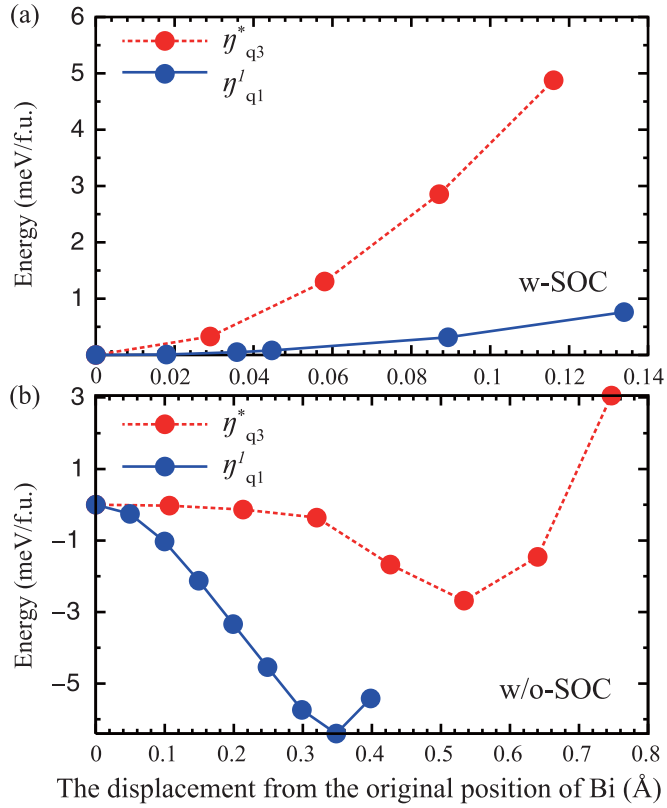

FIG. 4. Total energy variation as a function of atomic displacement for each phonon mode of La_2O_2Bi in the w-SOC (a) and w/o-SOC (b) schemes.

La_2O_2Bi are hardened substantially not to have imaginary phonon frequencies at the FS nesting $\mathbf{q}$ vectors. This feature indicates that the SOC suppresses the CDW instability in La_2O_2Bi. Namely, in La_2O_2Bi, the SOC reduces $\chi_0(\mathbf{q})$, which then becomes not large enough to yield $\omega_{\mathbf{q}} < 0$. Accordingly, our results certainly demonstrate that the disappearance of imaginary phonon frequency in La_2O_2Bi arises from the large SOC effect, whereas that in Er_2O_2Bi arises from the volume contraction due to smaller R atomic size.

To estimate the distortion-induced energy gain in La_2O_2Bi, we carry out total energy calculations as a function of atomic displacements given by the softened phonon modes in Fig. 3(a). We denote the corresponding normal mode at each $\mathbf{q}_i$ as $\eta^j_{\mathbf{q}_i}$, where j is the index of phonon mode having the lowest frequency at $\mathbf{q}_i$. We have also considered $\eta^*_{\mathbf{q}_3}$, which is a linearly superposed mode of nearly degenerate $\eta^1_{\mathbf{q}_3}$ and $\eta^2_{\mathbf{q}_3}$. $\eta^1_{\mathbf{q}_1}$ induces the Bi dimer formation along each x or y direction [1D-ladder type shown in Fig. 5(d)], while $\eta^*_{\mathbf{q}_3}$ induces the herringbone-type distortion [Fig. 5(b)]. In the w-SOC scheme of Fig. 4(a), both normal modes do not bring about the energy gains, which is consistent with no imaginary phonon frequency. Total energies for $\eta^1_{\mathbf{q}_3}$ and $\eta^2_{\mathbf{q}_3}$ are estimated to be higher than that for $\eta^*_{\mathbf{q}_3}$. Note that the energy loss for $\eta^1_{\mathbf{q}_1}$ is only about 0.7 meV for the displacement of Bi with 0.14 Å. This is consistent with the largest phonon softening at $\mathbf{q}_1$. This feature also suggests the possible structural dynamics even at room temperature, which gives rise to the vibration of Bi atoms along the x or y direction to have the Bi-Bi distance between

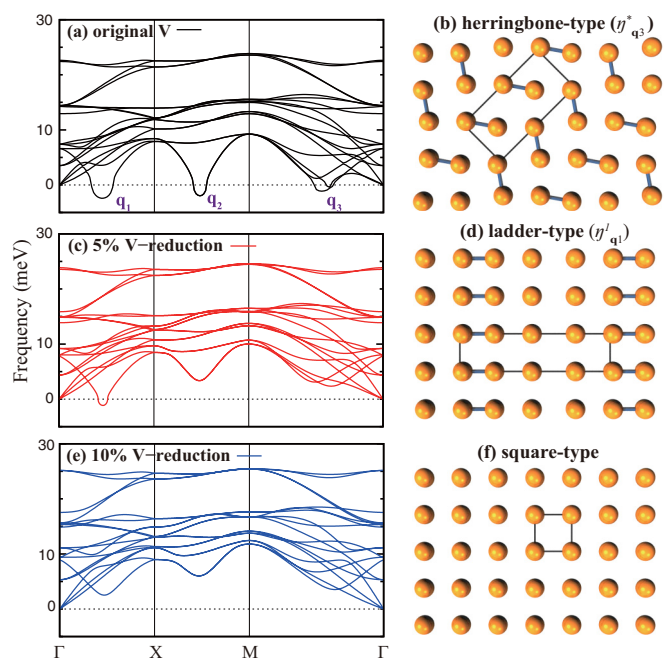

FIG. 5. (a) and (b) The phonon dispersion of Er_2O_2Sb with original volume and the most stable structure with normal mode $\eta^*_{\mathbf{q}_3}$. (c) and (d) The phonon dispersion of Er_2O_2Sb with 5% reduced volume and the most stable structure with normal mode $\eta^1_{\mathbf{q}_1}$. (e) and (f) The phonon dispersion of Er_2O_2Sb with 10% reduced volume and the stable square-type structure.

3.82 and 4.38 Å. This property also explains the experimental report on the apparent local disorder within the Bi layer [14].

As shown in Fig. 4(b), in the w/o-SOC scheme for La_2O_2Bi, $\eta^1_{\mathbf{q}_1}$ is the most stabilized mode. But, with applying the negative pressure (volume expansion of 3%), $\eta^*_{\mathbf{q}_3}$ becomes more stabilized to have a herringbone-type structure. On the contrary, upon pressure (volume contraction of 3%), only $\eta^1_{\mathbf{q}_1}$ has the energy gain. This feature indicates that $\eta^*_{\mathbf{q}_3}$ is more sensitive than $\eta^1_{\mathbf{q}_1}$ to the volume variation. In Er_2O_2Bi, which is equivalent to pressurized La_2O_2Bi, both normal modes do not have the energy gain, and so the Bi square sheet is retained. This suggests that, if the SOC is not considered, the Bi layer can be changed from herringbone type, to 1D-ladder type, and to a square sheet for negative, ambient, and positive pressure, respectively. It is noteworthy that R_2O_2Bi in the w/o-SOC scheme has a structural instability similar to R_2O_2Sb despite the difference in volume. The interesting point is that La_2O_2Sb is distorted into a herringbone type due to the phonon softening instability at $\eta^*_{\mathbf{q}_3}$ [10], even though the volume of La_2O_2Sb is smaller (0.6%) than that of La_2O_2Bi. This seemingly inconsistency is attributed to the substantial orbital overlap of the extended Bi $6p$ orbital as compared to the Sb $5p$ orbital. Namely, although Bi-Bi separation in R_2O_2Bi is larger than Sb-Sb separation in R_2O_2Sb, the spatially extended Bi $6p$ orbitals produce the volume contraction effect.

Then we examine the pressure effect on Er_2O_2Sb, which has the smaller volume. For this purpose we calculate the phonon dispersion with decreased volume, as shown in Fig. 5. In our previous work [10] we have shown that the phonon softening instability occurs at $\mathbf{q}_1$, $\mathbf{q}_2$, and $\mathbf{q}_3$ vector at the ambient pressure, as reproduced in Fig. 5(a). The most favorable mode in energy is a linearly superposed mode $\eta^*_{\mathbf{q}_3}$ showing the herringbone-type pattern [Fig. 5(b)]. With increasing pressure, the overall phonons become hardened due to the suppression of the FS nesting [10], and eventually the imaginary phonon frequencies disappear. As shown in Fig. 5(c), for 5% reduced volume, the phonon softening instabilities at $\mathbf{q}_2$ and $\mathbf{q}_3$ disappear, and only that at $\mathbf{q}_1$ remains. In this case, the Sb layer is distorted into an 1D-ladder type along the x or y direction [Fig. 5(d)], and the system would exhibit metallic behavior because of partial CDW gap opening. For the 10% reduced volume, all the phonon instabilities disappear, as shown in Fig. 5(e), and so the CDW instability is completely suppressed to retain the Sb square sheet with metallic nature.

We summarize in Fig. 6 the schematic structural behaviors of R_2O_2Sb and R_2O_2Bi under the real or chemical pressure. The CDW instability within Sb layer of R_2O_2Sb induces a herringbone-type distortion having an insulating phase with the full CDW gap. The CDW gap is to be reduced by the chemical pressure from La to Er. With applying the real pressure on Er_2O_2Sb, the favorable displacement mode changes from $\eta^*_{\mathbf{q}_3}$ to $\eta^1_{\mathbf{q}_1}$, and the insulating phase disappears. The distortion of $\eta^1_{\mathbf{q}_1}$ (1D-ladder type) opens only the partial CDW gap along the direction of the dimer, which is reduced by increasing the pressure. At last, the CDW instability disappears under high pressure, and the square sheet is retained with metallic behavior. In the w-SOC scheme of La_2O_2Bi, the CDW instability is suppressed by the SOC, so the square sheet is retained. Nevertheless, the local displacement of the Bi atom

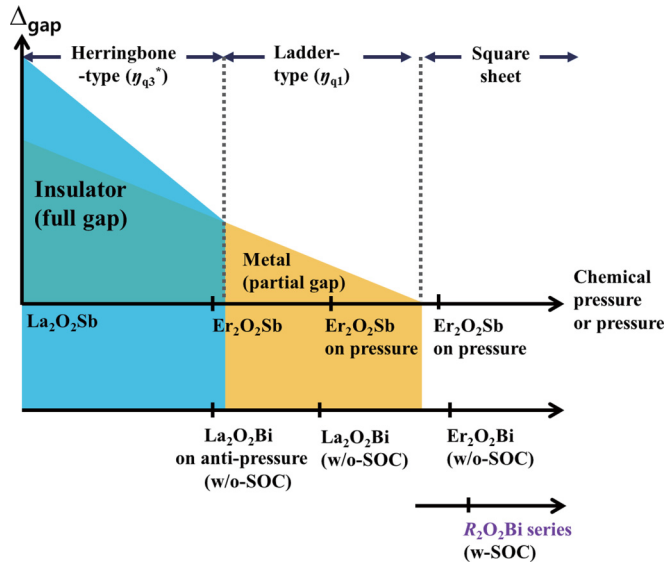

FIG. 6. Band gap versus pressure phase diagram of R_2O_2Sb and R_2O_2Bi.

along the x or y direction can exist dynamically due to the phonon softening close to zero frequency at $\eta^1_{\mathbf{q}_1}$. In Er_2O_2Bi, the dynamical instability is suppressed due to the volume contraction and orbital overlap of extended Bi $6p$ orbitals.

Now we inspect the resistivity behavior in La_2O_2Bi, which exhibits an anomalous upturn at low temperature. As mentioned earlier, a Mott-type insulator was invoked for this behavior by Mizoguchi and Hosono [7]. To check whether the Mott transition can be realized in La_2O_2Bi or not, we have performed the GGA+U ($U = 6$ eV) calculations for both La_2O_2Bi and Er_2O_2Bi. The resulting band structures for finite U on Bi p-orbital states do not show any signature of band gap opening. In fact, such behavior is expected in view of the very large bandwidth of Bi $6p$ states, as much as 4–5 eV. Thus, it is not plausible to invoke the Mott transition for the anomalous resistivity behavior in La_2O_2Bi.

Note that R_2O_2Bi in Fig. 3 has the soft phonon modes even in the absence of the structural instabilities. It is seen that the soft phonon frequencies in La_2O_2Bi are much lower in energy than those in Er_2O_2Bi, which in turn suggests that the EPC in La_2O_2Bi will be larger than that in Er_2O_2Bi. It is because the EPC is, in general, inversely proportional to the square of the phonon frequency. Then the stronger the EPC, the more the electron-phonon scattering occurs, which is expected to provide the slight increase in the resistivity in La_2O_2Bi, as in the small-polaron picture. This picture is interesting, remaining to be resolved in the future.

IV. CONCLUSIONS

We have investigated the electronic structures and phonon properties of R_2O_2Bi (R = La, Er) to explore the origin of the stable Bi^{2-} square sheets in these systems. The stable square sheet in La_2O_2Bi originates from the suppression of the CDW instability due to the large SOC of Bi $6p$ orbitals. On the other hand, the stable square sheet in Er_2O_2Bi originates primarily from the volume contraction due to small R atomic size in addition to the SOC effect. We have also examined the

pressure effect on R_2O_2Sb, which shows the structural change from herringbone type, to 1D-ladder type, and eventually to square sheet with increasing pressure, as is consistent with the behavior in R_2O_2Bi having the intrinsic chemical pressure effect. Furthermore, we have ruled out the Mott-type transition invoked for the anomalous resistivity upturn in La_2O_2Bi upon cooling. Instead, we suggest that it can be explained by the strong EPC, which arises from the existing soft phonon modes in La_2O_2Bi, as invoked in the small polaron picture.

ACKNOWLEDGMENTS

Helpful discussions with Sooran Kim are greatly appreciated. This work was supported by the National Research Foundation of Korea (Grants No. 2011-0025237, No. 2013M2B2A9A03051257, No. 2013R1A1A2006416, and No. 2015R1A2A1A15053564), Max-Plank POSTECH/KOREA Research Initiative, and KISTI (Grant No. KSC-2014-C3-044).

[1] A. M. Mills, R. Lam, M. J. Ferguson, L. Deakin, and A. Mar, Coord. Chem. Rev. **233–234**, 207 (2002).
[2] F. Hulliger and R. Schmelczer, J. Solid State Chem. **26**, 389 (1978).
[3] F. Hulliger, R. Schmelczer, and D. Schwarzenbach, J. Solid State Chem. **21**, 371 (1977).
[4] R. Wang, R. Bodnar, and H. Steinfink, Inorg. Chem. **5**, 1468 (1966).
[5] E. Brechtel, G. Cordier, and H. Schäfer, J. Less-Common Met. **79**, 131 (1981).
[6] J. Park, G. Lee, F. Wolff-Fabris, Y. Y. Koh, M. J. Eom, Y. K. Kim, M. A. Farhan, Y. J. Jo, C. Kim, J. H. Shim, and J. S. Kim, Phys. Rev. Lett. **107**, 126402 (2011).
[7] H. Mizoguchi, S. Matsuishi, M. Hirano, M. Tachibana, E. Takayama-Muromachi, H. Kawaji, and H. Hosono, Phys. Rev. Lett. **106**, 057002 (2011).
[8] Z.-M. Sun and J.-G. Mag, J. Solid State Chem. **177**, 3752 (2004).
[9] G. A. Papoian and R. Hoffmann, Angew. Chem. Int. Ed. **39**, 2408 (2000).
[10] H. Kim, C.-J. Kang, K. Kim, J. H. Shim, and B. I. Min, Phys. Rev. B **91**, 165130 (2015).
[11] O. V. Magdysyuk, J. Nuss, and M. Jansen, Acta Crystallogr. Sect. B **69**, 547 (2013).
[12] J. Nuss and M. Jansen, J. Alloys Compd. **480**, 57 (2009).
[13] P. L. Wang, T. Kolodiazhnyi, J. Yao, and Y. Mozharivskyi, J. Am. Chem. Soc. **134**, 1426 (2012).
[14] J. Nuss and M. Jansen, Z. Anorg. Allg. Chem. **638**, 611 (2012).
[15] H. Mizoguchi and H. Hosono, J. Am. Chem. Soc. **133**, 2394 (2011).
[16] G. Kresse and J. Furthmüller, Phys. Rev. B **54**, 11169 (1996); Comput. Mater. Sci. **6**, 15 (1996).
[17] P. Blaha, K. Schwarz, G. K. H. Madsen, D. Kavasnicka, and J. Luitz, *Wien2k* (Karlheinz Schwarz, Technische Universitat Wien, Austria, 2001).
[18] K. Parlinski, Z.-Q. Li, and Y. Kawazoe, Phys. Rev. Lett. **78**, 4063 (1997).
[19] A. Togo, F. Oba, and I. Tanaka, Phys. Rev. B **78**, 134106 (2008).
[20] G. Derrien, M. Tillard-Charbonnel, A. Manteghetti, L. Monconduit, and C. Belin, J. Solid State Chem. **164**, 169 (2002).
[21] V. Brouet, W. L. Yang, X. J. Zhou, Z. Hussain, R. G. Moore, R. He, D. H. Lu, Z. X. Shen, J. Laverock, S. B. Dugdale, N. Ru, and I. R. Fisher, Phys. Rev. B **77**, 235104 (2008).
[22] C.-J. Kang, K. Kim, and B. I. Min, Phys. Rev. B **86**, 054115 (2012).